Published online 28 September 2017

Nucleic Acids Research, 2017, Vol. 45, No. 22 ***e180***
doi: 10.1093/nar/gkx857

Arrayed mutant haploid embryonic stem cell libraries facilitate phenotype-driven genetic screens

Guang Liu[1,2,†], Xue Wang[1,2,†], Yufang Liu[1,2,†], Meili Zhang[1,2], Tao Cai[3], Zhirong Shen[3], Yuyan Jia[1,2] and Yue Huang[1,2,*]

[1]State Key Laboratory of Medical Molecular Biology, Institute of Basic Medical Sciences, Chinese Academy of Medical Sciences & Peking Union Medical College, Beijing 100005, China, [2]Department of Medical Genetics, Institute of Basic Medical Sciences, Chinese Academy of Medical Sciences & Peking Union Medical College, Beijing 100005, China and [3]National Institute of Biological Sciences, Beijing 102206, China

Received June 23, 2016; Revised August 22, 2017; Editorial Decision September 11, 2017; Accepted September 19, 2017

ABSTRACT

Forward genetic screens using mammalian embryonic stem (ES) cells have identified genes required for numerous cellular processes. However, loss-of-function screens are more difficult to conduct in diploid cells because, in most cases, both alleles of a gene must be mutated to exhibit a phenotype. Recently, mammalian haploid ES cell lines were successfully established and applied to several recessive genetic screens. However, all these screens were performed in mixed pools of mutant cells and were mainly based on positive selection. In general, negative screening is not easy to apply to these mixed pools, although quantitative deep sequencing of mutagen insertions can help to identify some 'missing' mutants. Moreover, the interplay between different mutant cells in the mixed pools would interfere with the readout of the screens. Here, we developed a method for rapidly generating arrayed haploid mutant libraries in which the proportion of homozygous mutant clones can reach 85%. After screening thousands of individual mutant clones, we identified a number of novel factors required for the onset of differentiation in ES cells. A negative screen was also conducted to discover mutations conferring cells with increased sensitivity to DNA double-strand breaks induced by the drug doxorubicin. Both of these screens illustrate the value of this system.

BACKGROUND

Loss-of-function genetic screens using mammalian cell lines are valuable tools to identify genes required for numerous cellular processes (1,2). Genome-wide libraries of homozygous mutant cells are the substrates for conducting these screens, but the diploid nature of mammalian genomes hampers the generation of these mutants. Given this disadvantage, large-scale genetic screens cannot be conducted as widely as those in yeast, *Drosophila* or *Caenorhabditis elegans*, in which genome-wide homozygous mutation libraries can easily be generated (3–5). We and others have previously reported methods to selectively isolate homozygous mutant cells from a mixed population of heterozygous and homozygous cells that were generated using a general Cre-loxP and gene trap-based mutagenesis strategy (6,7). Although homozygous mutants in hundreds of genes have been obtained, it is still a time-consuming and laborious task to create a genome-wide library of cells with null mutations. Recently, a near-haploid human leukemia cell line and its derivatives have been used to isolate loss-of-function mutants and to perform several genetic screens successfully (8–15). This cell line has great potential for functional genomics, but the phenotypes that can be screened are limited to those accessible in transformed lymphoid cells.

Mammalian embryonic stem (ES) cells retain unlimited self-renewal potential in culture and can be induced to differentiate into all somatic cell types under appropriate culture conditions. Thus, these cells offer powerful approaches to study gene function more widely than before (16,17). In 2011, two groups reported the isolation and establishment of haploid mouse ES cell lines (18,19) that resemble diploid ES cells in their proliferation and pluripotent capacity (20). Haploid ES cells were also applied to generate large pools of random mutations in combination with retroviral or transposon-based mutagenesis, and to conduct a few small- or large-scale genetic screens, including studies to identify genes responsible for resistance to lectin toxins and the clinical poly(ADP-ribose) polymerase inhibitor olaparib (19,21), the identification of factors driving the differentiation of ES cells (22), and the silencing factors involved in X chromosome inactivation (23). However, all these screens were performed in mixed pools of a vast num-

*To whom correspondence should be addressed. Tel: +86 10 69156462; Fax: +86 10 65256546; Email: huangyue@pumc.edu.cn
†These authors contributed equally to this work as first authors.

ber of mutant cells, indicating that the null mutants of interest must be selected either positively using a lethal drug or indirectly using an artificial cellular reporter construct. Recently, a genome-wide barcode transposon screen was used to identify drug-sensitive phenotypes, but the screen was still performed in mixed pools (24). Thus, the application of haploid ES cells in genetic screening remains limited. An arrayed clonal library of haploid ES cells, each with a different gene mutation, could certainly facilitate recessive genetic screens (25).

In this study, we use haploid ES cells and *piggyBac* (PB) transposons to construct arrayed homozygous mutant libraries rapidly, and we apply this technology to a positive genetic screen to identify 'exit-from-pluripotency' factors and to a negative genetic screen to identify mutations conferring increased sensitivity to the DNA double-strand break (DSB)-inducing drug doxorubicin. Moreover, the established arrayed mutation libraries can serve as open resources for a wide variety of phenotype-driven genetic screens. The method significantly expands the scope of genetic screening and facilitates functional studies of mammalian genomes.

MATERIALS AND METHODS

Cell culture

Haploid mouse ES cell line AGH-OG-3 (26) was kindly provided by Prof. Jinsong Li (Institute of Biochemistry and Cell Biology, Shanghai). The cell culture was modified from a previous study (27). The cells were cultured on γ-irradiated DR4 Mouse Embryonic Fibroblast (MEF) (28) feeder cells (neomycin, hygromycin, puromycin and 6-thioguanine-resistant) in ES Cell medium supplemented with 15% fetal bovine serum (FBS), 1000 U/ml leukemia inhibitory factor (LIF), 3 μM CHIR99021 and 1 μM PD0325901. The cells were cultured at 37°C with 5% CO_2 in a humidified environment. After 3–4 passages of culture, haploid ES cells were purified by fluorescence-activated cell sorting (FACS). The dissociated cells were incubated with 10 μg/ml Hoechst 33342 dye at 37°C for 30 min, and the haploid 1n peak was purified with a BD FACSAria II flow cytometer with an excitation wavelength of 407 nm (violet laser) for further culturing. Flow cytometric data were analyzed using BD FACSDiva software. Mouse diploid ES cell line AB1 and its derivatives were cultured on γ-irradiated MEF feeder cells in ES cell culture medium supplemented with 15% FBS and 1000 U/ml LIF. In all experiments, the cells were counted using a Scepter™ cytometer (Millipore).

Construction of PBDGTV vector

The PBDGTV vector was constructed based on the TNN vector previously described (6). First, the selection cassette was inversed by Cre recombinase *in vitro* (NEB), and it conferred the resistance to the drug puromycin. The cassette *neo-SV40 pA was* then deleted by restriction enzyme Psp XI (NEB). The 7.6 kb fragment was extracted using agarose gel and self-ligated using T4 DNA Ligase (NEB). The final vector was confirmed by restriction digestion and sequencing. This vector was named PBDGTV (*piggyBac* based Dual Gene Trap Vector), and full sequence of these vectors is available from GenBank under accession number (KU179219). The PBDGTV plasmid will be available from Addgene (#100859).

Embryoid body (EB) formation

EBs were formed from diploid ES cells AB1 as previously described (29). Briefly, cultured ES cells were dissociated with trypsin on the day of passage and sedimented for 30 min at 37°C. A total of 1.5×10^6 cells were transferred to low attachment 90-mm-diameter bacteriological-grade Petri dishes in differentiating medium containing knockout DMEM (KO-DMEM), 15% FBS, 2 mM GlutaMax, 1% non-essential amino acids (NEAA), and 100 μM β -mercaptoethanol. The cultures were replaced with fresh differentiation medium every other day. EBs were cultured for 10 more days.

Generation of the genome-wide arrayed mutant library

For mutagenesis, haploid ES cells with a high 1n peak were purified by FACS and were further cultured for 5–6 days. Ten million cells were transfected by electroporation (230 V, 500 μF; Bio-Rad Gene Pulser) with 1 μg PBDGTV transposon donor plasmid and 10 μg pCMV-hyPBase transposase expression plasmid. After electroporation, the cells were plated onto 90-mm feeder plates. Puromycin selection (3 μg/ml) was initiated 24 h later and continued for 5 days until individual ES cell clones were visible. The puromycin-resistant clones within each plate were pooled and expanded for 4 days to generate one library called the haploid *piggyBac* library (HPBL).

To generate the genome-wide mutant arrayed library, cells from one mutant pool were plated at a low density and selected against by puromycin (1.5 μg/ml) after 24–36 h. After clonal expansion, single clones were picked from each dish and plated onto 96-well plates for further culture. Each plate contained 92 mutant clones, and the four wells at the corners remained empty for plating positive (mTcf3$^{-/-}$-E9 and mTcf3$^{-/-}$-F6) and wild-type (AGH-OG-3) controls in the subsequent screening. When the cells were confluent, they were split at 1:3 and used for further screens. In this study, we plated and assessed the phenotypes and GFP expression manually. The arrayed haploid mutation libraries are available upon request from the BEIJING ZHONGYUAN LTD (http://www.sinozhongyuan.com/en/Article_Show.asp?ArticleID=652) repository.

Splinkerette PCR to identify the transposon insertion sites

The Splinkerette-PCR method to identify the transposon insertion sites was the same as that as previously described (6). Briefly, genomic DNA was extracted, digested and ligated with the corresponding Splinkerette adaptors HMSp-*Sau*3A I (generated by annealing Splinkerette oligos HMSpBb-*Sau*3AI with HMSpAa), followed by two rounds of nested PCR.

DNA library preparation for Illumina

The optimized protocol for DNA library preparation for Illumina based on two methods was the same as that previously described (30,31). Ten micrograms of genomic DNA

from each mixed library was sheared by focused sonication with a fragment size of ∼200–400 bp using the Covaris sonication system (Covaris S220). The fragmented DNA was purified using AMPure XP beads and analyzed on a 2% agarose gel to examine the fragment sizes. The fragmented DNA was distributed with a peak at ∼300 bp. We used the NEBNext Ultra DNA Library Prep Kit for Illumina (NEB) to repair the ends of these fragments. We added 3'dA overhangs and ligated the fragment with Splinkerette T-overhang linkers (generated by annealing Splinkerette oligos SplkTp with SplkTm). Then, the junction fragments for the 3′ and 5′ ends of the *PiggyBac* transposon (PB3' ITR and PB5' ITR) were amplified in two consecutive Splinkerette PCR rounds to generate PB3 and PB5 libraries for each pool. Approximately 750 ng of adaptor-ligated DNA was used in the subsequent junction-fragment enrichment. In the first round of PCR, a Splinkerette adaptor specific primer Sp-1 and primer PB5-1 or PB3-1 that was specific for the PB5' ITR or PB3' ITR, respectively, were used. The reaction volume was 25 μl, and the annealing temperature was 60°C for 30 PCR cycles. In the nested PCR round, 0.5 μl of the first-round PCR product was used as the template. Primer P5-Sp-2 contained terminal adapter sequences (P5) for Illumina solid-phase amplification and sequencing and a Splinkerette adaptor-specific sequence. Primer PB5-2.a or PB3-2.a contained sequences for Illumina sequencing and a specific sequence for the PB5' ITR or PB3' ITR accordingly. Other primers P7-PB-2.b*n* ($n = 1$, 2, 3, or 4) contained terminal adapter sequences (P7) for Illumina solid-phase amplification, and a 6-base bar code followed by 13 bp that overlapped with the 5′ terminal sequence of primers PB5–2.a or 3′ counterpart PB3–2.a accordingly. The PCR reaction volume was 50 μl, and the final concentration of the P5-Sp-2, PB5-2.a (or PB3-2.a) and P7-PB-2.bn primers were 1 μM, 2 nM and 1 μM, respectively. The PCR cycling conditions included an initial annealing temperature of 50°C for 2 cycles, followed by an annealing temperature of 60°C for 18 cycles. Two Illumina DNA libraries of each HPBL based on PB3 and PB5 were generated, and a size selection of 300–500 bp for fragmented DNA was performed using AMPure XP beads following the manufacturer's instructions. These libraries were sequenced on a single lane of an Illumina HiSeq2000 device at BGI with pair-end reads of 2 × 100 bases read lengths following the manufacturer's recommended conditions. The PhiX DNA was added to libraries to increase complexity for Illumina sequencing. The customized PB5-ITR sequencing primer SP-read1 for read 1, Read2_primer for read 2 and an indexing sequencing primer Index_primer were used to decode the barcode of each library. Raw sequences were grouped into eight bins based on the barcode sequences incorporated into primer P7-PB-2.b*n*, and each barcode library included two paired-end read files. The primer and adapter sequences are listed in Supplementary Table S2.

Bioinformatic analysis

For the high-throughput libraries, the read pairs were trimmed of adapters and PB tags before mapping to the genome using a FASTX-toolkit (http://hannonlab.cshl.edu/fastx_toolkit/commandline.html) with the default parameter. The PB tag (TATCTTTCTAGGGTTAA) was removed from the 5′ end of the first mate with a custom script, and the adapter sequence (ACTAGTGGT) was removed from the 3′ end of the first mate, requiring an overlap of at least 3 nt. For the corresponding mate, the PB sequence was removed from the 3′ end. The trimmed paired end reads were aligned to the mouse reference genome (mm10) with Bowtie 2 software (http://bowtie-bio.sourceforge.net/bowtie2), allowing two mismatches and selecting unique alignments. In the case of the identification of an identical integration site in independent screens, we considered it a potential cross-contamination and assigned it to the library where it exhibited the largest number of reads.

Negative screen on the arrayed mutant library

The primary high-throughput screens were conducted in 384-well plates. We passaged the arrayed mutant haploid cell clones, which were cultured in 96-well plates, to 384-well plates at a relative low cell density using the PIPETMAX 268 automated liquid handling platform (Gilson) to ensure the identity between duplicate wells. Thus, each mutant clone has four repeat wells in a 384-well plate. Twenty-four hours later, cells in half of the wells were treated with 0.01 μg/ml doxorubicin. Eight hours later, the culture medium was changed to M15L without the drug. Seventy-two hours later, the cells were stained with Hoechst 33342 (10 μg/ml, Sigma) to identify the nucleus. The AGH-OG-3 haploid cells contained the Oct4-EGFP transgenic fragment, so the fluorescence intensity of GFP reflected the cell viability. The cells were imaged and analyzed by a fluorescence-based Cellomics ArrayScan high-content screening (HCS) Reader (Thermo Fisher) using the Morphology Explorer BioApplication. The optical fields were scanned with a 10 × objective lens to obtain the total number of cells per well. Hoechst 33342 stained and GFP images were acquired using the 386/23 nm excitation and 460/40 nm emission filters or 485/20 nm excitation and 535/50 nm emission filters respectively. We employed *Z*-score analysis to determine the potential candidate clones that became increased sensitivity to doxorubicin. Next, a validation screen of these candidate clones was conducted in 48-well plates with graded concentrations of doxorubicin, and cell viability was also detected by the HCS Reader.

Z-scores were calculated using the formula: $z = (X - \mu)/\text{s.d.}$, where X is the sample value calculated according to the number of surviving cells treated with doxorubicin divided by the number of cells without doxorubicin treatment, μ is the mean value and s.d. is the standard deviation of the entire population of one 96-well plate (32).

Reverse transcription PCR and quantitative real-time PCR

Total RNA was extracted from ES cells and EBs using TRIzol reagent (Invitrogen). One microgram of total RNA was reverse transcribed using the PrimeScript 1st Strand cDNA Synthesis Kit (TaKaRa). cDNA was analyzed by PCR using Premix Taq (TaKaRa) according to manufacturer's instructions. For the mutant gene expression, PCR primers were custom-designed to flank the insertion site of the gene-trap cassette. A real-time PCR reaction was performed in triplicate using Fast SYBR® Green Master Mix

(Applied Biosystems) and run on a StepOne Plus Real-Time PCR System (Applied Biosystems). The primer sets used are listed in Supplementary Table S3. The amount of ACTB expression was used to normalize all values.

PBase reversal

Five million mutant ES cells were electroporated with 20 μg *piggyBac* transposase expression plasmid, and were plated onto 90-mm feeder plates. Two days later, the cells were re-plated at low density (1000 cells/90-mm plate) to allow the growth of individual ES cell colonies. Clones were picked into 96-well plates and the deletion of the PB transposon was confirmed by PCR.

CRISPR/Cas system mediated-gene knockout in mouse ES cells

To destroy the function of a candidate gene, we disrupted the common exons within all transcripts. The sgRNA-specifying oligo sequences spanning genes were chosen to minimize the likelihood of off-target cleavage using publicly available online tools (http://crispr.mit.edu/) and following the protocol described by Zhang's laboratory (33,34). The sequences with the highest scores were chosen. A 'G' was added to the 5′ end of the sgRNA that contained no 'G' to ensure optimal expression from the U6 promoter. *Tcf3*$^{-/-}$ ES cell lines were established using the CRISPR/Cas system in the haploid ES cell line. Two sgRNAs targeting exon 1 and exon 2 were designed to disrupt exon 2 of *Tcf3*. The annealed oligos were cloned into pX330 to construct the recombinant plasmid. The two pX330-sgRNA plasmids for each gene and a puromycin-selection plasmid, PB-puro, were co-electroporated into AGH-OG-3 ES cells. After 48 h of puromycin-selection, electroporated cells were trypsinized and replated to allow the growth of ES cell colonies. ES cell colonies were picked on day 7. Genomic DNA was extracted from the cells, and PCR was performed to analyze the targeted clones. PCR products were further sequenced to confirm the knockouts. Of the 96 cell clones that were genotyped using the PCR assay, 16 clones carried a homozygous deletion of *Tcf3,* and 12 clones were heterozygous mutations. Potential off-target analysis was performed as previously described (35). Two homozygous mutants, mTcf3$^{-/-}$-E9 and mTcf3$^{-/-}$-F6, were selected for further study.

To minimize off-target cleavage, we further employed a double-nicking strategy using the Cas9 nickase (D10A) (36) mutant with paired guide RNAs to disrupt candidate genes, including *Garnl3, Sema5a, Pde3a, Ifltd1*, *Cadps, Cdk5rap2, Phf21a* and *Gapt,* in the AB1 ES cells. The sgRNAs were cloned into the pX335 construct that expressed Cas9 nickase (D10A). Gene knockout clones were identified by enzyme digestion of the PCR product combined with Sanger sequencing. The sequences between each paired sgRNA contained an enzyme site and could be digested by the corresponding enzyme. When the paired sgRNAs induced NHEJ at the target site, the enzyme site was lost, and the length or number of cleavage bands was altered. The PCR products were cloned into pMD18-T vectors (TaKaRa) and sequenced. The oligos and primers are listed in Supplementary Table S2.

Alkaline phosphatase staining

Five days after plating, the cells were fixed with 4% paraformaldehyde for 2 min, washed in a rinse buffer, and stained with the Leukocyte Alkaline Phosphatase Kit (Sigma) following the manufacturer's instructions. The positive colonies were counted using an inverted microscope (Olympus, X41). For AP staining after LIF withdrawal, 'undifferentiated' means AP-positive cells only, 'partially differentiated' indicates a mixture of AP-positive and -negative cells, and 'totally differentiated' represents AP-negative cells only. These criteria have been used previously (37,38).

Statistical analysis

The data are presented as the means ± S.D. A two-tailed Student's *t*-test was used to analyze the significance. $P < 0.05$ was considered significant. Data analyses were performed using GraphPad Prism software.

RESULTS

Generation and characterization of haploid genome-wide mutant libraries

To generate a genome-wide mutant library, we used the haploid mouse ES cell line AGH-OG-3 (26), which contains the Oct4-EGFP transgenic fragment, and gene-trap vector PB-DGTV (P*iggy*B*ac* transposon based D*u*al directional G*e*ne T*r*ap V*e*ctor) to disrupt transcription (Figure 1A). PB transposons have high chromosomal integration efficiencies in ES cells and exhibit less bias for genomic hot spots compared with retroviral vectors (39). This vector contains the selection marker gene *puroΔTK* that is driven by the mouse phosphoglyceratekinase promoter (PGK), and which allows selection for PB integration into the chromosome using puromycin. In this vector, the mutagens are two non-selectable gene-trap cassettes that contain two pairs of terminal exons with their preceding introns from *Ccdc107* and *Dom3z* in opposing orientations. Several premature stop codons in each reading frame were inserted into each penultimate exon, which should cause 'loss-of-function' of the trapped genes (6). Unlike the classical promoter trap that required the expression of the target genes for the selection of clones, PBDGTV can be used for the selection of mutant clones independent of target gene expression.

At electroporation, the AGH-OG-3 ES cells remained primarily haploid after a few passages, and were subject to flow sorting (Supplementary Figure S1). Using conditions that achieve on average one transposon insertion per cell (39), we electroporated ten million AGH-OG-3 cells with 1 μg PBDGTV and 10 μg hyperactive PB transposase (PBase) (40) to generate four independent mutant libraries (HPBL1–HPBL4) containing 15 000–20 000 puromycin-resistant colonies each (Figure 1B). The transposon copy number was determined by Southern blot analysis on dozens of individual clones randomly picked from the HPBL1 library using a restriction enzyme that generates a unique transposon–host junction fragment for each transposon integration site (Figure 1C). The majority of these cell clones contain a single-copy insertion of the transposon.

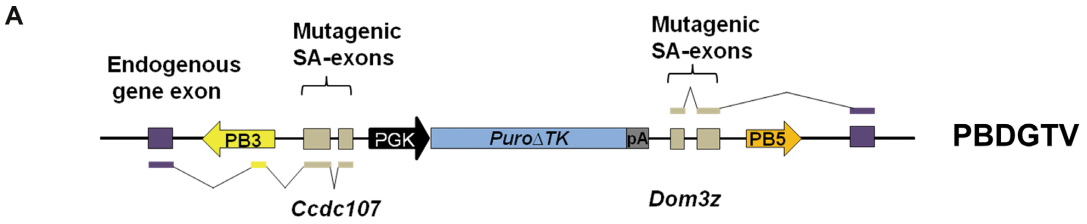

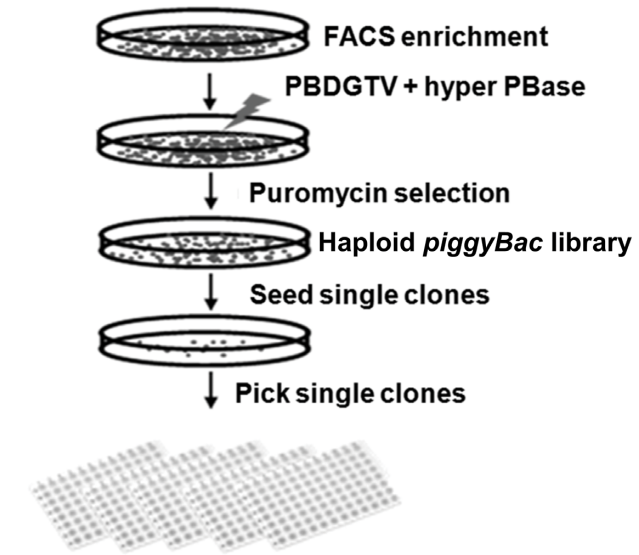

D

	Number
Reads	2,575,569
Insertion	63,684
Intergenic	28,426 (44.6%)
In genes	35,258 (55.4%)
Mutated genes	18,497

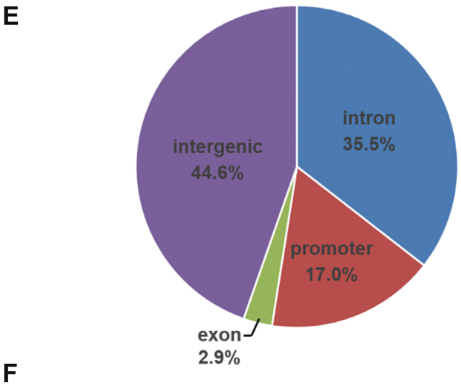

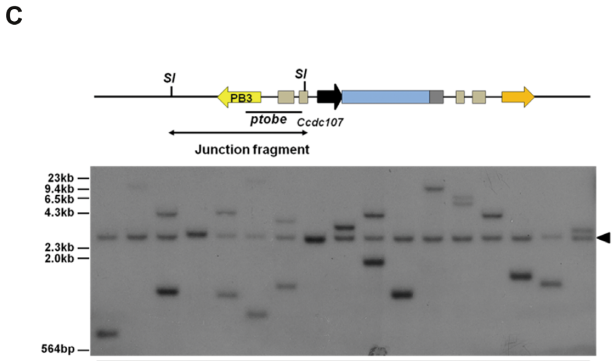

Number of clone				
Copy number per clone				Percentage of single copy
1	2	3	>3	
35	11	1	0	74

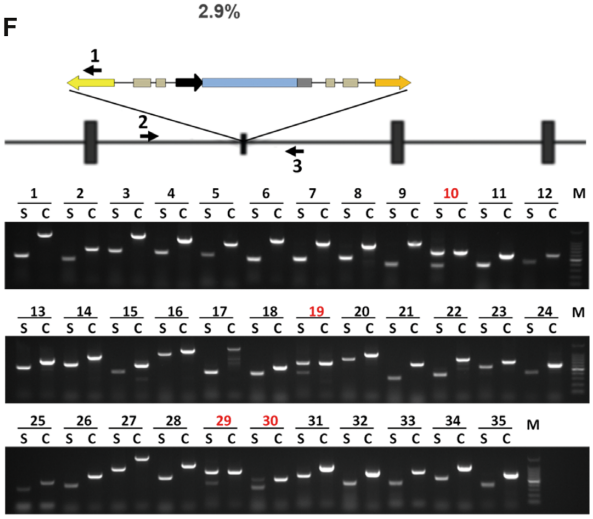

Figure 1. Generation and characterization of the mutant haploid ES cell library. (**A**) Structure of the vector PBDGTV for gene trap. The vector is shown integrated into an intron, with purple boxes representing exons of the disrupted gene. PBDGTV can trap genes transcribed in either direction. SA, splice acceptor; PB5 and PB3, *PB* repeats; pA: SV40 ploy A; *Dom3z* and *Ccdc107*: mutagenic units with the terminal and penultimate exons of each gene. (**B**) The experimental scheme to generate the arrayed mutant haploid ES cell library. (**C**) Southern blot analysis of gene-trap clones reveals the host/transposon junction fragment in each clone. *SI*: *Stu* I; probe, a 550-bp PCR fragment from PB3 and *Ccdc107* in PBDGTV. Black triangles indicate the endogenous *Ccdc107*. The lower table is the summary of copy number per clone in the arrayed library. (**D**) The distribution rates of PB (*piggyBac*) transposon in the mutant library. The transposon landed in 45% intergenic and 55% intragenic regions, with a high frequency of integration into introns. (**E**) Splinkerette PCR combined with massively parallel sequencing to identify the genome coverage and distribution rates of PB transposon in the mutant library. (**F**) Homozygosity analysis of individual mutant ES cell clones. S, mutant sample; C, wild-type haploid ES cells, AGH-OG-3. Heterozygous mutants are marked by red color.

To explore the genomic coverage of these libraries, we used Splinkerette-PCR combined with massive parallel sequencing (30,31), which is a method employed to specifically isolate and sequence transposon-host junctions, to assess the overall mutants present in the mutation libraries (Supplementary Figure S2). We unambiguously identified 63 684 insertions. Approximately 45% of these insertions were mapped to intergenic regions, and ∼55% of the insertions occurred in intragenic regions and promoter regions, encompassing 18 841 different genes in total (Figure 1D and E). The genome distribution of the PB transposon was similar to that previously reported for diploid ES cells (41). Taken together, these data indicate that HPBLs are an eligible resource for the generation of arrayed homozygous mutant ES cell clones.

Construction of an arrayed haploid mutation library

To generate an arrayed mutant library, cells from HPBL1 were plated at a low density for clonal expansion, and several thousand individual clones were picked and cultured on 96-well plates (Figure 1B). Three copies of the large-scale mutation library were cryopreserved in liquid nitrogen. At this stage, most clones have a diploid DNA content due to inherent spontaneous diploidization of haploid ES cells (data not shown).

To investigate the percentage of homozygous mutations in the arrayed mutant library, we selected cell clones with single-copy PB insertions, identified the transposon-host junction in these clones and performed PCR analysis with site-specific primers separately. Of the 35 individual cell lines analyzed, thirty-one clones (>85%) carried homozygous insertions (Figure 1F). This result also indicated that most transposon insertions occurred in haploid cells.

'Exit-from-pluripotency' screens using the arrayed mutation library

Using the arrayed mutation library established from the haploid pluripotent stem cells, we conducted recessive screens to identify the factors that promote 'exit-from-pluripotency' in ES cells. In the screening, we used a T-cell factor 3 (Tcf3)-null ES cell line as the positive control. Tcf3 (encoded by *Tcf7l1*) is a member of the Tcf protein family (Tcf1, Tcf3, Tcf4 and Lef1 in mammals), which is a DNA-binding transcriptional regulator of the canonical Wnt signaling pathway (42). Previous studies have demonstrated that the *Tcf3* deletion caused ES cells to be refractory to differentiation in culture (42,43). In our study, we used the powerful CRISPR/Cas system (33,44) to knockout Tcf3 in the haploid ES cell line AGH-OG-3 (Figure 2A). Two homozygous mutants, mTcf3$^{-/-}$-E9 and mTcf3$^{-/-}$-F6, were selected for further study (Figure 2b). We plated 2×10^4 *Tcf3*$^{-/-}$ ES cells onto a 24-well plate under ES cell-culture conditions. The following day, we switched to differentiation-permissive cultures, including a serum-containing medium (M15) without LIF or N2B27 medium, which induce the heterogeneous non-neural differentiation or neural differentiation of ES cells separately (45,46). After 3 days, *Tcf3*$^{-/-}$ cells still retained the ES cell colony morphology and were refractory to differentiation compared with the wild-type (WT) haploid ES cells (Figure 2C). None of the predicted off-target regions were mutated by CRISPR/Cas9 in the two cell clones (Figure 2D).

The primary high-throughput screens (92 clones/96-well plates, 22 plates in total) were conducted in 96-well plates under the two different differentiation-permissive conditions (Figure 3A). Three days later, the majority of these cell clones had differentiated like WT haploid cells do, but 151 individual mutant clones and *Tcf3*$^{-/-}$ cells still exhibited the ES cell colony morphology and expressed GFP at a relatively high level under one or both conditions. We extracted genomic DNA from these undifferentiated clones and identified the PB transposon insertion sites in the clones by Sp-PCR followed by sequencing. Eighty-eight insertions could be mapped to the reference mouse genome (GRCm38.p3), and 40 of them are located in encoding genes (Figure 3B, C and Supplementary Figure S3A). Among them, some genes were related to transcriptional regulation and mammalian development, and information regarding these genes is presented in Supplementary Table S1. Of these mutants, 36 clones were homozygous mutations, and 4 clones were heterozygous mutations, as determined by PCR analysis using site-specific primers (Figure 3D and Supplementary Figure S3B). The transposon copy numbers in the 88 mapped clones were also detected, and 65 clones harbored a single-copy PB insertion (Supplementary Figure S4). To investigate whether the gene-trap cassette was efficient and the transcripts of trapped genes were disrupted, we randomly selected seven cell clones, in which the trapped genes had relatively high expression levels in the WT ES cells. The primer pairs specific for the exons flanking the gene-trap insertion site were designed and used to amplify cDNA from the selected clones (Figure 4A). In all tested clones, including three Ccdc107 mutagen unit-trapped clones and four Dom3z mutagen unit-trapped clones, the expected fusion transcripts could be detected (Figure 4B), and the endogenous transcripts of trapped genes were effectively disrupted (Figure 4C).

Among these candidate 'exit-from-pluripotency' factors, we noticed that the two genes, *Smg1 and Kdm6a* (also known as *Utx*) have been previously implicated in ES cell differentiation. SMG1, a PI3K-related kinase, was identified in a large-scale small interfering RNA (siRNA) screen for differentiation regulators (47). Smg1-deficient mice died on embryonic day 8.5 (E8.5) (48), and knockdown of Smg1 in ES cells also inhibited their differentiation (49). KDM6A is a histone H3-lysine 27 demethylase that plays a critical role in the mesoderm differentiation of ES cells (50). KDM6A was also identified in genetic screening of the mixed pools of haploid mutants mentioned above. *Pde3a* encodes a phosphodiesterase that degrades the second messenger cyclic AMP (cAMP) (51). cAMP signal activation can functionally replace OCT4 to induce pluripotency (52), which is consistent with an earlier report that the cAMP agonist Forskolin was identified as a chemical 'substitute' for Oct4 in reprogramming (53). In addition, *Ubtf* was identified in both our screen and the mixed pool-based screen.

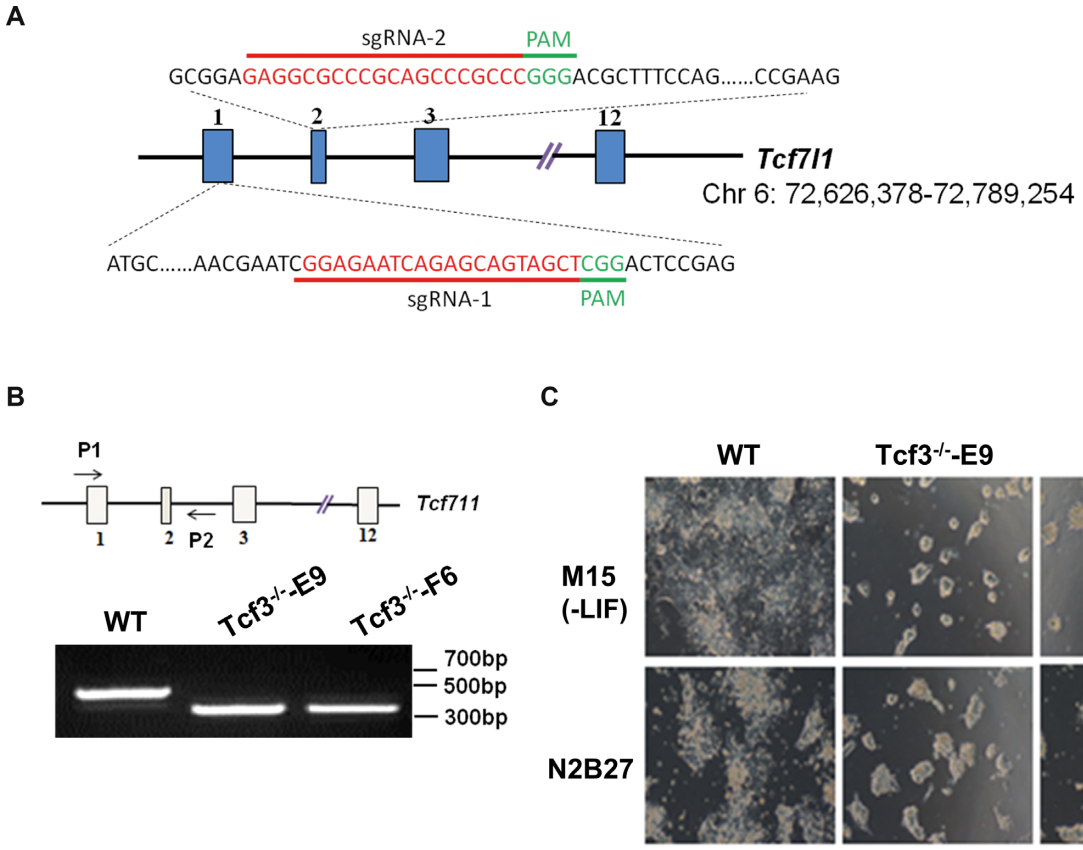

D

Potential off-target sites (sgRNA exon2)	Gene	Sequence(5'-3')	Target	
			E9	F6
Chr16: 76,351,589-76,373,049	NM_173440	GAGCCGGCCCCAGCCCGCCCGAG	NO	NO
Chr12: 57,230,446-57,497,199	NM_001164370	GGGTGGCCTGCAGCCCGCCCGGG	NO	NO
Chr14: 48,446,393-48,512,135	NM_172600	GAGGCGCGCACAGCCCGCGCCGG	NO	NO
Chr 3: 96,181,151-96,195,521	NM_022030	GAGACGCTGACAGCCCGCCCTGG	NO	NO
Chr 19: 46,137,032-46,140,983	NM_008852	AGGGCGCCCCCAGCCCGCCGCAG	NO	NO
Chr5: 31,054,928-31,078,232	NM_023525	GTGGGGTCGGCAGCCCGCCCGGG	NO	NO
Chr 18: 21,127,201-21,300,138	NM_001033445	GACGCCTGCGCAGCCCGCCCCGG	NO	NO

Figure 2. Create *Tcf3*$^{-/-}$ ES cell lines by CRISPR/Cas9 system. (**A**) Strategy to create *Tcf3*$^{-/-}$ cell lines by CRISPR/Cas9 system in AGH-OG-3 ES cells. The sgRNA-targeting sequence is labeled in red, and the protospacer-adjacent motif (PAM) sequence is labeled in green. (**B**) Identify *Tcf3*$^{-/-}$ cells by genomic PCR. WT: wild-type ES cells, AGH-OG-3; P1, P2: the primers. (**C**) The morphology of *Tcf3*$^{-/-}$ cells under differentiation conditions (M15 (-LIF) and N2B27). (**D**) Identification of the potential off-targets of CRISPR-Cas9 in *Tcf3*$^{-/-}$ clones.

Transposon excisions rescued differentiation deficiency in mutant cells

To establish the causality between transposon insertion mutations and the differentiation-deficiency phenotype, we removed the PB mutagen by re-expressing PBase in mutant ES cells. We randomly chose 8 mutant clones with intragenic PB insertion to conduct the reversibility analysis. Both homozygous and heterozygous revertants were obtained from five mutant cell lines. However, only heterozygous revertants were isolated for the other three mutant lines (Table 1, Figure 5A and Supplementary Figure S5A). The WT transcripts of five mutated genes, *Garnl3, Sema5a, Pde3a, Cdk5rap2* and *Cadps*, can be detected in these revertants (Figure 5B and Supplementary Figure S5B). The expression of the other three genes was very low in the WT ES cells. Thus, even in the revertants, the transcripts cannot be detected (data not shown). We then tested the differentiation ability of these homozygous and heterozy-

A

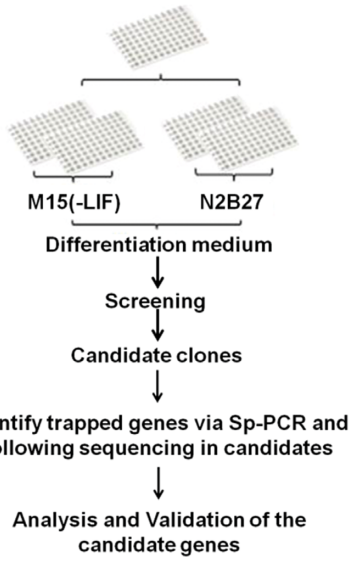

B

Screening 2,024 clones			
Positive clones number	Splinkerette PCR sequence	Mapped to reference genome	Overlapping genes
151	113	88	40

C

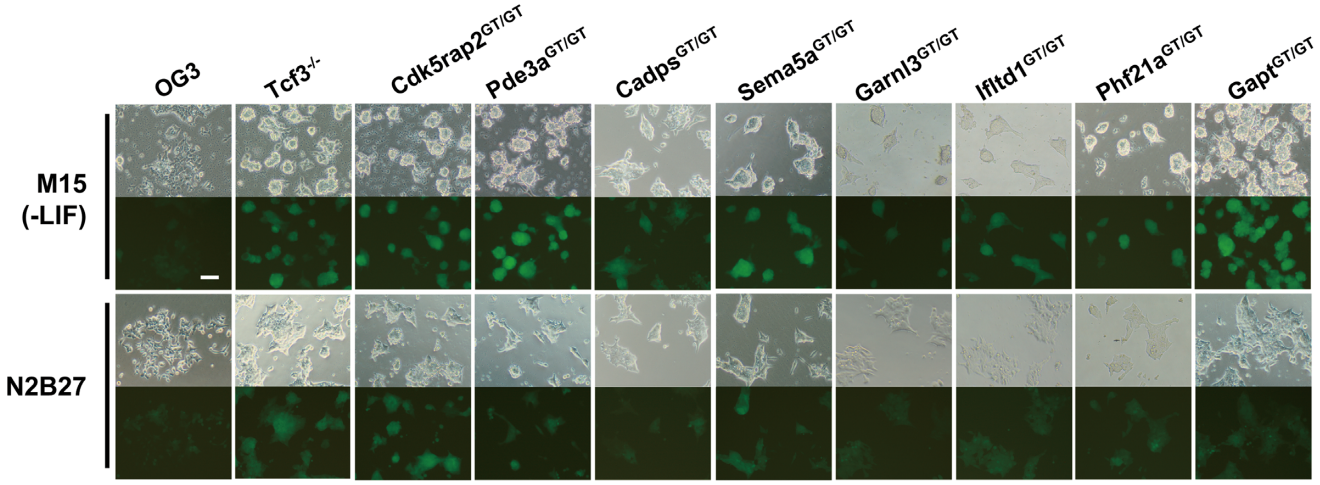

D

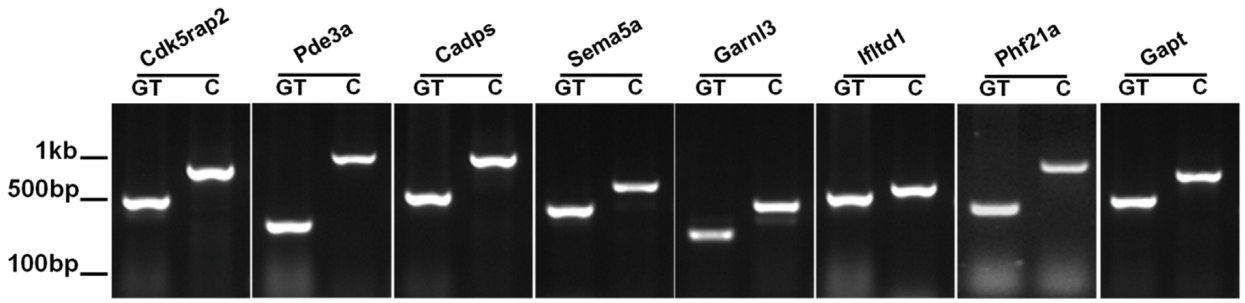

Figure 3. Using the arrayed mutant haploid ES cell library to screen the mutant clones with differentiation defects. (**A**) The schematic screening procedure using the arrayed mutant library. Each screen contained duplicated wells. (**B**) Summary of the screening covering 2,024 clones. (**C**) Representative morphologies of differentiation defects of several mutant clones under differentiation culture conditions. OG3: wild-type haploid ES cells, AGH-OG-3; *Tcf3*$^{-/-}$ ES cells were as the positive control of differentiation defects; GT: gene trap, scale bar, 100 μm. Full data are available in Supplementary Figure S3. (**D**) Triple-primer genomic PCR of candidates detected the transposon/host junctions with the expected size. The representative candidate clones lacked the WT band, consistent with being homozygous mutants. Primers 1, 2 and 3 (shown in Figure 1F) were used. GT: gene trap, C: wild-type ES cells, AGH-OG-3.

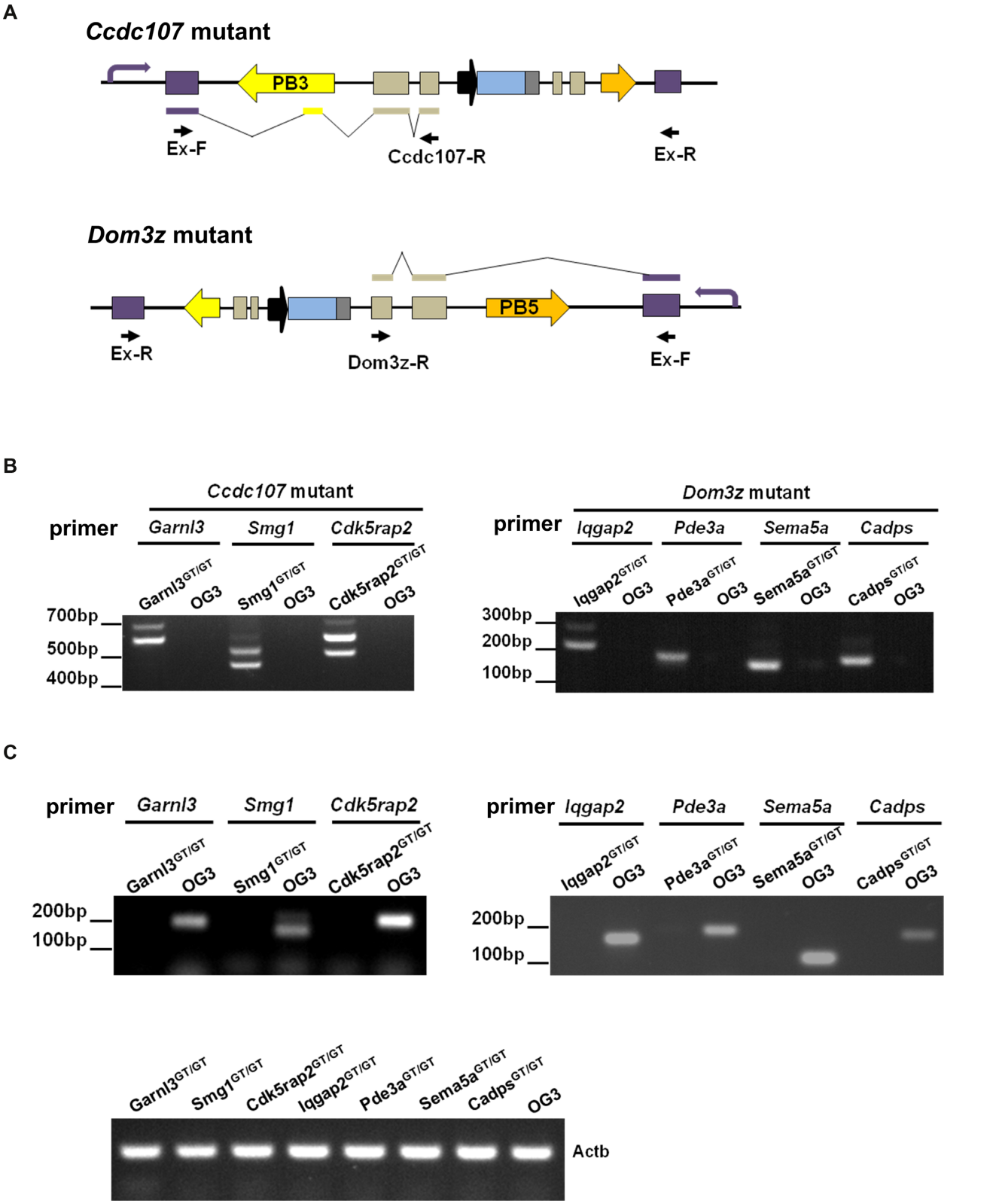

Figure 4. Characterization of the trapping events mediated by the mutagenic units. (**A**) The trapping characteristics of the mutagenic units. Primers for the Ccdc107 or Dom3z in PBDGTV and upstream exonic primer of insertion site of mutant genes detected fusion transcripts; Ex-F, Ex-R: exonic PCR primers flanking the integration sites. (**B**) The expression of fusion transcripts in the gene-trap mutants with *Ccdc107* and *Dom3z* mutagenic unit. GT: gene trap, OG3: WT ES cells, AGH-OG-3. (**C**) RT-PCR confirmed that the expression of these genes was abolished in the corresponding gene-trapping clones. Exonic PCR primers flanking the integration sites are indicated on the upper part of the upper panel. Actb is an internal control.

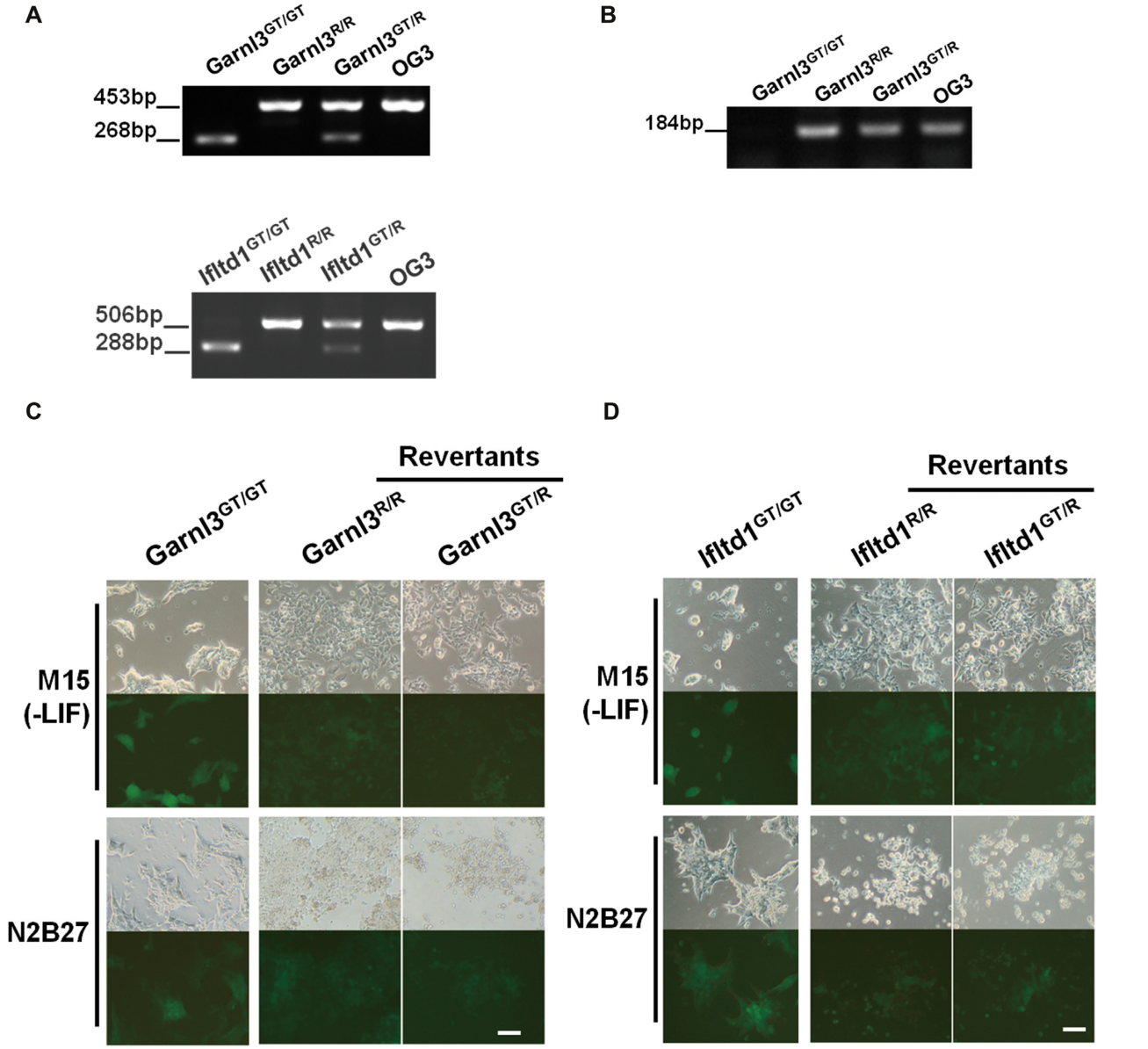

Figure 5. Reversibility analysis of the mutant clones with differentiation defects. (**A**) Genotyping of PBDGTV insertion in *Garnl3 and Ifltd1*. The WT fragment was absent in the original mutant clone $Garnl3^{GT/GT}$ *and* $Ifltd1^{GT/GT}$, but amplified from the two revertants ($Garnl3^{R/R}$, $Garnl3^{GT/R}$) of each mutant clone. The primers for mutant (Junction) and WT alleles were used. GT: gene trap, R: revertants. (**B**) RT–PCR showing loss of WT transcript of *Garnl3* in $Garnl3^{GT/GT}$ and the amplification of transcript in $Garnl3^{R/R}$, $Garnl3^{GT/R}$ and AGH-OG-3 cells. The transcript of Ifltd1 was not detected in the origin mutant clone ($Ifltd1^{GT/GT}$) and two revertants ($Ifltd1^{R/R}$, $Ifltd1^{GT/R}$). (**C** and **D**) Morphologies of $Garnl3^{GT/GT}$ and $Ifltd1^{GT/GT}$ and their revertants under differentiation culture conditions. It is indicated that revertant clones regained differentiation abilities. Scale bar, 100 μm.

gous revertants. Under the differentiation condition, the homozygous or heterozygous revertant subclones of six mutant genes regained their differentiation ability, including *Garnl3* (Figure 5C), *Ifltd1* (Figure 5D), *Sema5a, Pde3a, Phf21and Cadps* (Supplementary Figure S5C). Heterozygous revertant clones of $Gapt^{GT/GT}$ displayed a partial recovery differentiation phenotype under the condition of differentiation N2B27, and $Cdk5rap2^{GT/GT}$ also exhibited a lower degree of the recovery differentiation phenotype under the M15 (-LIF) differentiation condition (Supplementary Figure S5C). Partial recovery from differentiation deficiency in some heterozygous revertants might indicate dosage-sensitive activity of these mutated genes. These results demonstrated that the differentiation-resistant phenotype was caused by the insertion of the PB transposon, and most, if not all, of the candidate genes identified from the genetic screen on the arrayed mutation libraries were likely to cause the observed phenotype.

Validation of selected 'exit-from-pluripotency' genes in diploid ES cells

To further verify these newly discovered differentiation inducers and to exclude any effects specific to the genetic background of the haploid ES cell line, we used

Table 1. The selected mutant clones for reversibility analysis

NO	Symbol*	Insertion site	Location	Mutagen	Reverse	
					Homozygous	Heterozygous
1	Garnl3(–)	2:33010478	intron18	*Ccdc107*	4/96	8/96
2	Pde3a(+)	6:141472033	intron6	*Dom3z*	1/96	5/96
3	Sema5a(+)	15:32432477	intron1	*Dom3z*	1/96	3/96
4	Ifltd1(Lmntd1)(–)	6:145524640	Upstream of exon1	*Dom3z*	13/96	7/96
5	Phf21a(+)	2:92202856	Upstream of exon1	*Dom3z*	3/96	11/96
6	Cadps(–)	14:12812550	intron1	*Dom3z*	0	2/96
7	Cdk5rap2(–)	4:70398941	intron3	*Ccdc107*	0	6/96
8	Gapt(–)	13:110340974	11.6 kb	*Ccdc107*	0	10/96

*: +, forward strand; –, reverse strand.

CRISPR/Cas9 technology to delete critical exons of these genes in the diploid AB1 ES cell line, which has been widely used in mouse genetic studies in recent decades. Then, we investigated the onset of the differentiation of these gene-knockout ES cells. To minimize the possible off-target cleavages, we conducted a double-nicking strategy using the Cas9 nickase with paired guide RNAs (36). The sgRNA-specifying oligo sequences are presented in Figure 6A and Supplementary Figure S6. For all eight candidate genes mentioned above, homozygous mutant ES cell clones were identified by digesting the genomic PCR product with the appropriate restriction enzymes (Figure 6B and Supplementary Figure S7A) and DNA sequencing (Supplementary Figure S7B).

We examined the proliferation abilities of AB1 and AB1-derived mutant ES cells in culture, and most cell lines exhibited rapid proliferation except for the slightly slower growth of the *Ifltd1*-null cell line (Supplementary Figure S8A). Flow cytometry-based cell cycle analysis revealed no difference between the WT and mutant ES cells (Supplementary Figure S8B), although some mutant ES cells mildly affected the expression of the apoptosis marker Annexin V (Supplementary Figure S8C). To determine whether gene mutations affect the differentiation capacities of ES cells under LIF withdrawal, we cultured the WT and mutant ES cells in M15 (-LIF) medium. The colonies were scored as undifferentiated, partially differentiated or totally differentiated based on AP staining. Most of the WT ES cells rapidly progressed to partial or total differentiation, whereas the mutant ES cells formed more AP-positive colonies after LIF withdrawal for 5 days except *phf21a* (Supplementary Figures S8D and E).

EB formation has been proposed as a model for early embryonic development in terms of differentiation capacity, morphological changes, and inductive signaling events that drive these changes (54). To further assess the differentiation capacity of these mutant cell clones, we cultured them in suspension to promote EB formation. At early stage, all eight mutant ES cell lines could aggregate and form EB-like structures. Then, most of the WT AB1 cell-derived EBs formed cystic structures at day 8 and beyond, whereas six mutants generated more compact and/or smaller EBs. *Pde3a*-null and *Cadps*-null cell-derived EBs have structures that are cystic but smaller than the WT structures (Figure 6C and Supplementary Figure S9A). The expression levels of the ES cell marker gene *Oct4* (also known as *Pou5f1*) were reduced more slowly in the mutant EBs at the indicated time points of differentiation, except in two gene mutations: *Cadps*-null and *Cdk5rap2*-null cells (Figure 6D and Supplementary Figure S9B). Moreover, the expression of three germ layer-specific marker genes was also detected during EB formation. For each mutant, one or more marker genes were aberrantly expressed compared with the WT AB1 cells. For instance, *Garnl3* mutant ES cells aberrantly expressed the mesoderm marker gene Brachyury and the endoderm marker gene AFP at different time points of EB formation. In *Ifltd1* mutant ES cells, the up-regulation of AFP was reduced and significantly lower than the WT levels (Figure 6E). *Sema5a*-null and *Cdk5rap2*-null ES cells aberrantly expressed FGF5 at an early stage and delayed the up-regulation of AFP levels. Other mutant genes also decreased the up-regulation of the expression of more than one marker, except in the case of *Cadps* and *Phf21a* (Supplementary Figure S9C). Taken together, these results indicated that all tested genes except *Cadps* are necessary for the onset of ES cell differentiation.

A negative screen for factors conferring increased sensitivity to doxorubicin using the arrayed mutation library

To demonstrate the advantages of the established arrayed mutation libraries on 'negative selection'-based screens, we performed a negative screen to identify factors conferring cells with the increased sensitivity to the DNA-damaging drug doxorubicin (DOX), which is also known as Adriamycin. DOX is an anticancer drug widely used in the clinic; however, drug resistance has compromised its efficacy (55) (Figure 7A). First, we titrated the drug concentration, cell density and detection time to be used in the high-throughput screens. Seventy-two hours after DOX withdrawal, the cell viability of different cell densities was between 50–65% at 0.01 μg/ml DOX, and the drug sensitivity of AGH-OG-3 cells was not influenced by the tested cell densities (Supplementary Figure S10). Thus, 0.01 μg/ml DOX and a cell density of 400–2400 cells/well were used in the following negative screens, and cell viability was detected at 72 h after the drug was withdrawn.

Then, the primary high-content screens (HCS) were conducted on 1152 mutant ES cell clones (96 clones/96-well plate, 12 plates in total). Among them, 21 candidate mutant clones were scored with negative stringency (Z-score < -2 in two duplicate experiments) (Supplementary Table S2a). Next, the validation screen of these 21 clones was conducted in 48-well plates with graded concentrations of DOX: 0, 0.01, 0.015 and 0.02 μg/ml. Thirteen candidate clones were ultimately confirmed (Figure 7B, Supplementary Figure S11 and Table S2B). We identified the PB transposon insertion sites in these clones. Eight insertions could

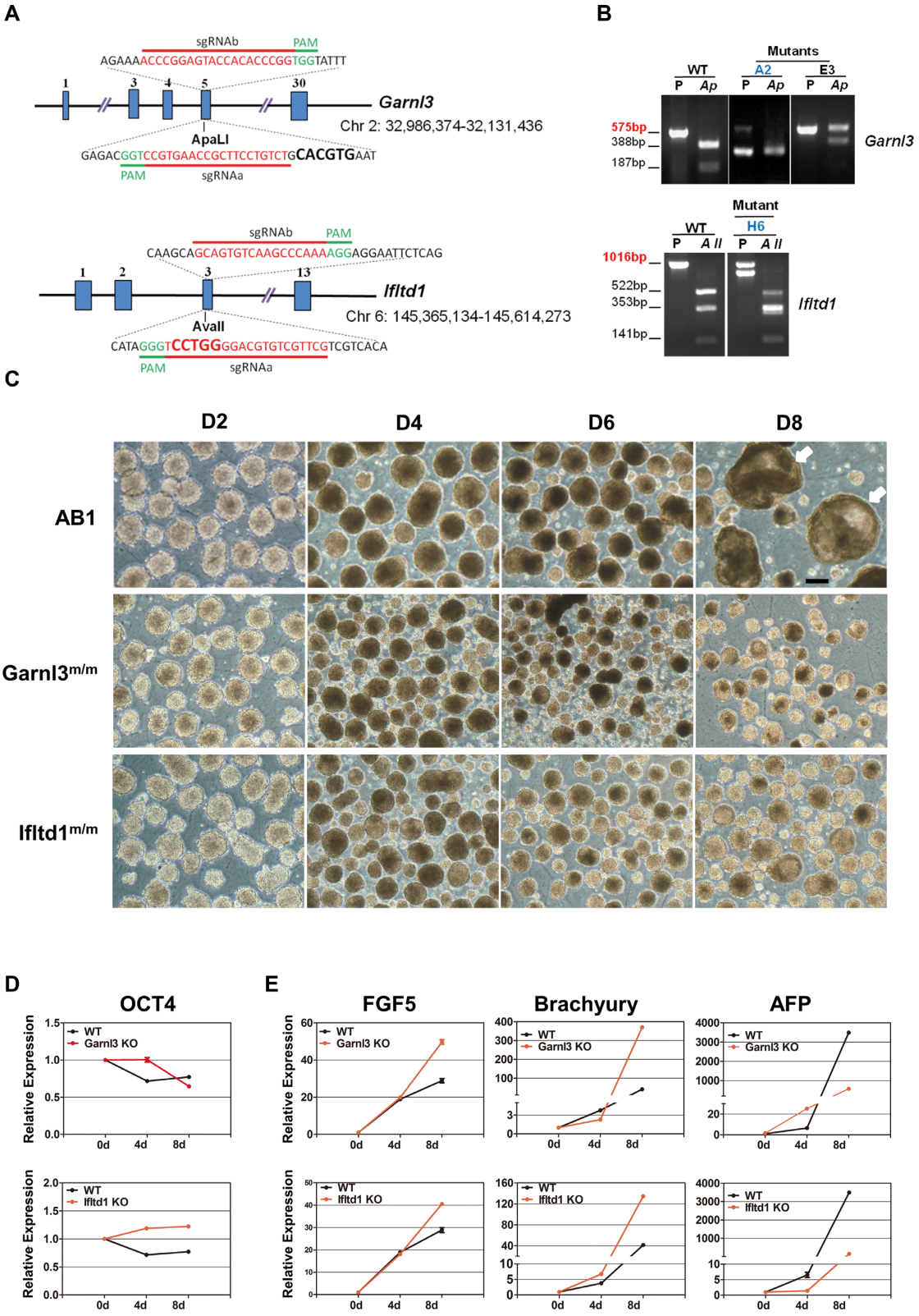

Figure 6. Limited differentiation of diploid ES cells with gene mutation. (**A**) Schematic of the Cas9/sgRNA-targeting sites in *Garnl3* and *Ifltd1*. The sgRNA-targeting sequence is labeled in red, and the protospacer-adjacent motif (PAM) sequence is labeled in green. The restriction sites at the target regions are in bold. (**B**) Genotyping of the mutant clones of *Garnl3* and *Ifltd1*. *Garnl3* PCR products were digested with ApaLI, and *Ifltd1* PCR products were digested with AvaII. The sequencing results of PCR products were shown in Supplementary Figure S7; the blue labeled mutant clones were used for EB formation. WT: wild-type ES cells, AB1; P: PCR product; *Ap*: *ApaL* I; *A II*: *Ava* II. (**C**) EB formation of mutant clones of *Garnl3* and *Ifltd1*. Most WT ES cell-derived EBs at day 8 of differentiation formed cystic structures (white arrows), whereas mutant ES cell derived EBs were more compact. Scale bar, 200 μm. (**D**) Time-course analysis of *Oct4* expression in WT and knockout ES Cell-derived EBs (*Garnl3* and *Ifltd1*). The data are shown as the mean. (**E**) Real-time PCR analysis of several lineage differentiation markers expression during EB formation. The data are shown as the mean ± S.D. ($n = 3$).

A

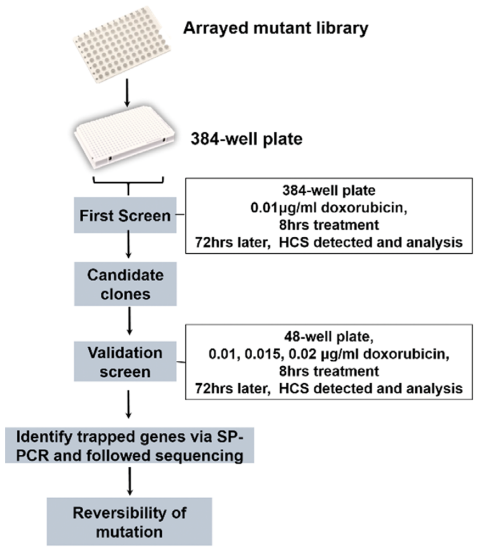

B

Screened 1152 clones

Candidate clones number (1st Screen)	Candidate clones number (Validation Screen)	Splinkerette PCR sequence	Mapped to reference genome	Overlapping genes
21	13	11	8	6

C

Mutated genes list

No.	Symbol#	Insertion site	Location	Mutagen	Gene Name*	Clone ID
1	**Rmi2(+)**	16:10853039	intron1	*Dom3z*	RecQ mediated genome instability 2	NS-1D1
2	**Acbd6(+)**	1:155612791	intron4	*Dom3z*	acyl-Coenzyme A binding domain containing 6	NS-2H1
3	**Hhat(-)**	1:192521613	intron11	*Ccdc107*	hedgehog acyltransferase	NS-5A6
4	**Pdk4(-)**	6:5485629	intron10	*Dom3z*	pyruvate dehydrogenase kinase, isoenzyme 4	NS-9F11
5	**Sfi1(-)**	11:3142152	intron21	*Ccdc107*	Sfi1 homolog, spindle assembly associated (yeast)	NS-10A10
6	**Sgk1(+)**	10:21983097	intron2	*Dom3z*	serum/glucocorticoid regulated kinase 1	NS-11H1

#: +, forward strand; -, reverse strand
*: These data come from MGI (Mouse Genome Informatics) database

Figure 7. Conducting a negative screen on the arrayed mutant libraries. (**A**) The schematic screening procedure using the arrayed mutant library. In the negative screens, we intended to identify factor whose lose would make cells become increased sensitivity to the DNA damaging drug doxorubicin. (**B**) Summary of the negative screening covering 1,152 clones. The data of primary and validation screen is on the Supplementary Table S2. (**C**) Mutated genes list of the negative screening. NS: Negative Screen. Clone ID: Location of the mutant clone on the 96-well plate.

be mapped to the reference mouse genome (GRCm38.p3), and 6 of them were located in encoding genes (Figure 7B and C).

To establish the causality between transposon insertion mutations and the increased DOX-sensitivity phenotype, PB mutagens were removed by re-expressing PBase in these six mutant ES cells. We successfully obtained revertants of three mutated genes: *Rmi2, Pdk4,* and *Acbd6* (Figure 8A). These revertant cell lines were subsequently exposed to DOX for 8 h and subjected to colony formation assays. As expected, the increased DOX sensitivity was not observed in these revertants (Figure 8B and C).

DISCUSSION

We have described a method for rapidly generating arrayed mutant ES cell libraries using haploid murine ES cell lines and PB transposon-based dual directional insertional mutagens. In the libraries, the proportion of homozygous mutant clones can reach 85%, and most clones contain a single-copy transposon insertion. These key features allow the arrayed mutant libraries to be applicable for high-throughput phenotypic screening. To explore their utility, we conducted a positive screen for recessive mutations that could confer differentiation resistance and a negative screen for mutations conferring increased doxorubicin sensitivity to cells. Both of the screens identified some genes, including known factors and several new candidates. Using transposase-mediated reversion analyses and/or rigorous CRISPR/Cas9-based loss-of-function assays in diploid ES cells, we validated some of these candidates, and the high confirmation frequency demonstrated the availability and high efficiency of genetic screens on the arrayed mutation libraries. Although RNAi-based gene knockdown and the newly developed CRISPR/Cas9 system can also be applied to construct arrayed mutant libraries (56,57), the variable gene-disruption efficiencies of different hairpin RNAs or the required 3–6 guide RNAs for one gene increase the number of individual mutant clones that constitute the library and thus compromise the application of these libraries. Moreover, the off-target effects associated with RNAi technology and the CRISPR/Cas9 system (58–60) also entangle the causal linkage between the phenotype and the targeted genes, which can be easily established in our screen system through direct transposase-mediated reversion analysis of candidate mutants.

Haploid ES cells largely resemble the nature of diploid pluripotent stem cells and thus serve as a versatile mammalian cell model. Recently, the near-haploid leukemia cell line KBM7 has been used to successfully conduct various genetic screens, including identifying host factors for the Influenza virus (8), Ebola virus (9), Lassa virus (61), Picornavirus (15) and bacterial toxins (62); revealing modifiers of position-effect variegation (11); and discovering proteins that are related to chemotherapy drug-mediated DNA damage (63). Given the cell identity and genomic instability of KBM7 cells, haploid ES cells should have a broader application in genetic screening, such as the one for 'exit-from-pluripotency' factors shown here, which obviously cannot be conducted on KBM7 cells. Moreover, targeted mutations or reporter constructs can easily be introduced into haploid ES cells (19,24,26,27), which should be beneficial

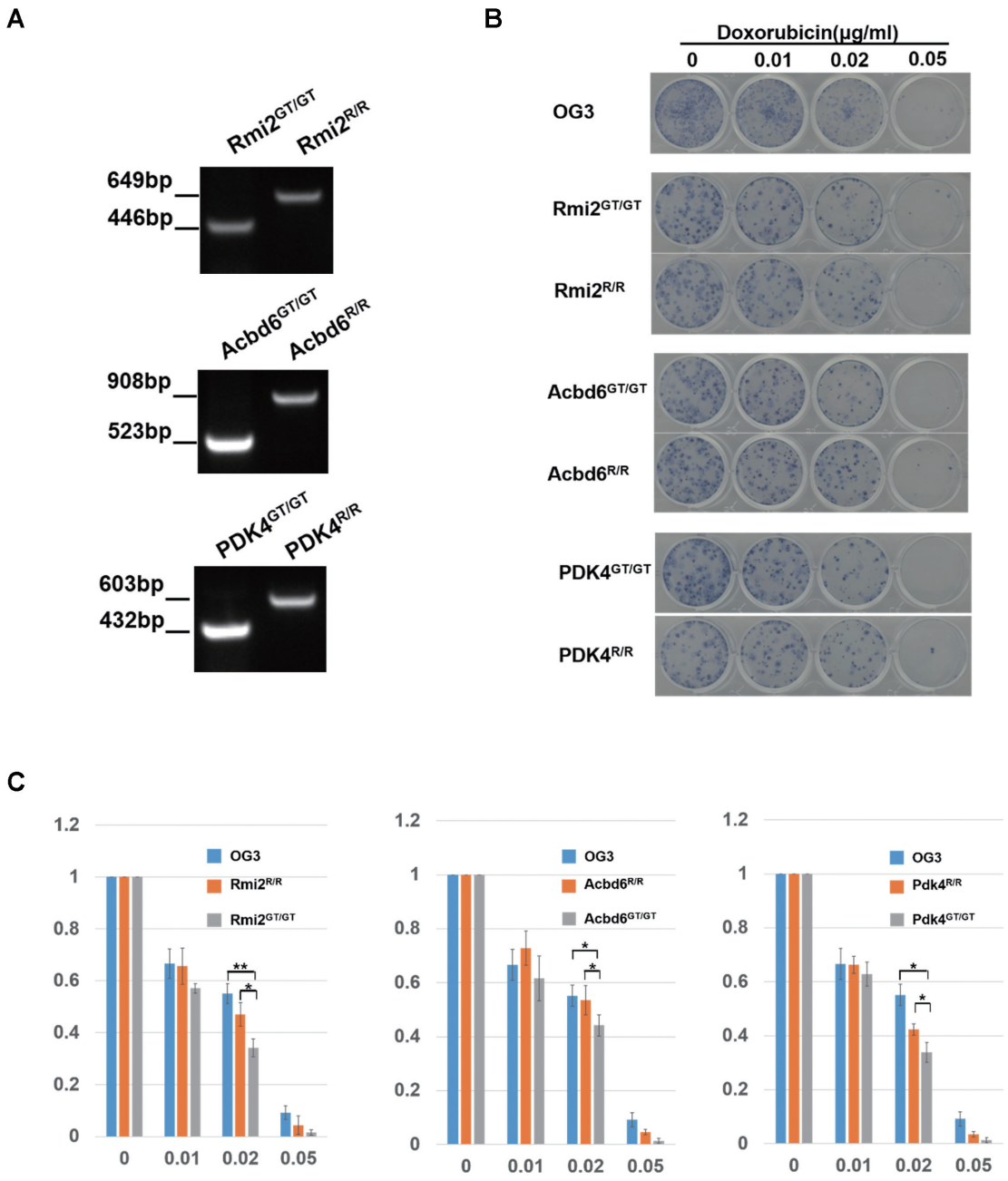

Figure 8. Reversibility analysis of the mutant clones with increased DOX sensitivity. (**A**) Genotyping of PBDGTV insertion in *Rmi2, Acbd6* and *Pdk4*. The WT fragment was absent in the original mutant clone $Rmi2^{GT/GT}$, $Acbd6^{GT/GT}$ and $Pdk4^{GT/GT}$, but amplified from the three revertants ($Rmi2^{GT/GT}$, $Acbd6^{GT/GT}$ and $Pdk4^{GT/GT}$) of each mutant clone. The primers for mutant (Junction) and WT alleles were used. GT: gene trap, R: revertants. (**B**) Morphologies of $Rmi2^{GT/GT}$, $Acbd6^{GT/GT}$ and $Pdk4^{GT/GT}$ and their revertants under doxorubicin treated. Cells were treated with the indicated concentration doxorubicin for 8 hours and left to grow out. After 6 days, cells were fixed, stained, and imaged. (**C**) Quantification of colony numbers per plate and condition from three independent experiments (±S.D.) of the images.

for designing more precise genetic screens. For example, via the knock-in of a well-defined lineage-commitment reporter into haploid ES cells before the construction of arrayed mutant libraries, specific differentiation regulators for a particular cell type could be identified.

Understanding the regulatory network of stem cell differentiation is critical for the use of stem cells in regenerative medicine. Here, we uncovered new differentiation regulators by screening thousands of arrayed haploid mutants. Compared with two previously reported genome-wide screens for 'exit-from-pluripotency' factors, including an RNA interference (RNAi) screen covering ∼10 000 coding genes (47) and a haploid screen of a mixed pool of mutations (22), our pilot screen does not exhibit a high overlap with their readouts (Supplementary Figure S12). Our finding agrees with previous discussions regarding different genetic

screening systems (25) and illustrate the value of the established arrayed mutation libraries. Obviously, ongoing expansion of the arrayed mutant libraries could increase the screening readout. Among these newly identified 'exit-from-pluripotency' genes, some genes are involved in embryonic developmental processes, and their inactivation leads to embryonic or neonatal lethality in knockout mice.

The initial evidence for the role of Sema5A in embryogenesis was demonstrated by the expression of Sema5A in specific regions of mouse embryos, demarcating distinct compartments of the developing somites or the undifferentiated neuroepithelium (64). The *Sema5a*-null mice died between E11.5 and E12.5 (65), and the complexity of the hierarchically organized branches of the cranial cardinal veins was decreased (66). These results indicate an essential role of Sema5A during embryonic development. PHF21A (PHD finger protein 21A) is a component of the BRAF–HDAC complex (BHC) involved in the transcriptional repression of neuron-specific genes in non-neuronal cells. *Phf21a* knockout mice die within 1 day of birth, and the lethality likely results from an inability to suckle properly and to take in milk (67). The function of *Phf21a* in early mouse ES cell differentiation was also identified using DNA microarray data (68). CDK5RAP2 is highly expressed in embryonic neural progenitors. *Cdk5rap2* mutant mice rarely survive beyond 1 week of age with disproportionately smaller brains both prenatally and at birth (69). *Cdk5rap2*-depleted mouse ES cells exhibit a severe proliferation defect and apoptosis during neural differentiation (70).

Currently, almost all reported genetic screens that are based on mixed mutant pools must rely on strong positive selections and the enrichment of resistant clones. In general, 'negative selection'-based screens are not easy to apply to these mixed pools. However, quantitative deep sequencing of mutagen insertions in the library before and after the screen, so-called PhITSeq, can help to identify some 'missing' mutants (71). More importantly, the interplay and interferences between different mutant cells in the mixed pools disturb the readouts of genetic screens. The arrayed haploid mutant libraries are applicable for negative screens, which are of interest for many biological questions (25,72). Here, we conducted a negative screen to identify mutants conferring cells with increased sensitivity to DOX, a frequently used chemotherapeutics drug to treat a wide spectrum of tumors through generating DNA double-strand breaks (DSB). Despite its broad applicability, drug resistance constitutes a serious clinical limitation of DOX. After the screening, we identified several DSB and DNA repair related genes. Among these genes, some are involved in DOX-related cytotoxicity.

Rmi2 was identified as a novel BLM complex-associated protein and can form a complex with BLM, topoisomerase III alpha and RMI1 (73,74). Deletion of RMI2 in patient and cell lines causes genome and chromosome instability phenotypes (75). Pdk4 (pyruvate dehydrogenase lipoamide kinase isozyme 4) is an inhibitor of the glycolytic enzyme PDH. PDK4 expression was elevated in a tamoxifen-resistant cell line (TamR-MCF-7), and the cells were cross-resistant to fulvestrant and doxorubicin (76). SGK1 is a stress-induced survival factor and exerts anti-apoptotic effects during doxorubicin induced nephrotic syndrome. In $sgk1^{-/-}$ mice, more severe apoptosis was noted following doxorubicin treatment, with rapid loss of renal cells thereafter (77). In addition, microarray analysis of MG-63 osteoblastic cells revealed that NMT2 (*N*-myristoyltransferase 2) is potentially involved in doxorubicin resistance (78). Another report demonstrated that the NMT stimulatory effect requires interaction with ACBD6 (acyl-CoA binding protein, acyl-CoA binding domain 6) and was enhanced by binding of ACBD6 to its ligand (79). Thus, our arrayed mutant libraries provide a useful tool for negative screens.

Overall, this study provides a practical and versatile platform for a wide variety of phenotype-driven genetic screening studies. Moreover, other mutations or reporter constructs can easily be introduced into the haploid ES cells to create customized libraries for more sophisticated screens. Therefore, our method significantly expands the scope of genetic screens and future functional studies in mammalian cells.

DATA AVAILABILITY

Splinkerette- PCR combined with massively parallel sequencing data from this study have been submitted to the NCBI Sequence Read Archive (SRA; http://www.ncbi.nlm.nih.gov/sra) under accession number SRP068129. The full sequence of PBDGTV (piggyBac based Dual Gene Trap Vector) vector is available from GenBank under accession number (KU179219). The PBDGTV plasmid will be available from Addgene (#100859).

SUPPLEMENTARY DATA

Supplementary Data are available at NAR Online.

ACKNOWLEDGEMENTS

We thank Li Cheng and Lihong Sun for technical assistance; Dr Jinsong Li (CAS) for providing haploid ES cell lines; Dr Allan Bradley (the Wellcome Trust Sanger Institute) for kindly providing AB1 ES cell line and hyper-*PB* transposase expression plasmid (pCMV-hyPBase). The PBDGTV plasmid will be available from Addgene (#100859) via the standard materials transfer agreement. The arrayed haploid mutation libraries are available upon request from the BEIJING ZHONGYUAN LTD (http://www.sinozhongyuan.com/en/Article_Show.asp?ArticleID=652) repository.

FUNDING

National Key Research and Development Program of China [2016YFA0100103 to Y.H.]; CAMS Innovation Fund for Medical Sciences [2016-I2M-3-002 to Y.H.]; National Key Basic Research Program of China [2013CB967002 to Y.H.]; National Natural Science Foundation of China [31671410 to Y.H.]. Funding for open access charge: National Key Research and Development Program of China; CAMS Innovation Fund for Medical Sciences; National Key Basic Research Program of China; National Natural Science Foundation of China.

Conflict of interest statement. None declared.

REFERENCES

1. Moresco,E.M., Li,X. and Beutler,B. (2013) Going forward with genetics: recent technological advances and forward genetics in mice. *Am. J. Pathol.*, **182**, 1462–1473.
2. Hardy,S., Legagneux,V., Audic,Y. and Paillard,L. (2010) Reverse genetics in eukaryotes. *Biol. Cell*, **102**, 561–580.
3. Forsburg,S.L. (2001) The art and design of genetic screens: yeast. *Nat. Rev. Genet.*, **2**, 659–668.
4. Jorgensen,E.M. and Mango,S.E. (2002) The art and design of genetic screens: caenorhabditis elegans. *Nat. Rev. Genet.*, **3**, 356–369.
5. St Johnston,D. (2002) The art and design of genetic screens: Drosophila melanogaster. *Nat. Rev. Genet.*, **3**, 176–188.
6. Huang,Y., Pettitt,S.J., Guo,G., Liu,G., Li,M.A., Yang,F. and Bradley,A. (2011) Isolation of homozygous mutant mouse embryonic stem cells using a dual selection system. *Nucleic Acids Res.*, **40**, e21.
7. Horie,K., Kokubu,C., Yoshida,J., Akagi,K., Isotani,A., Oshitani,A., Yusa,K., Ikeda,R., Huang,Y., Bradley,A. *et al.* (2011) A homozygous mutant embryonic stem cell bank applicable for phenotype-driven genetic screening. *Nat. Methods*, **8**, 1071–1077.
8. Carette,J.E., Guimaraes,C.P., Varadarajan,M., Park,A.S., Wuethrich,I., Godarova,A., Kotecki,M., Cochran,B.H., Spooner,E., Ploegh,H.L. *et al.* (2009) Haploid genetic screens in human cells identify host factors used by pathogens. *Science*, **326**, 1231–1235.
9. Carette,J.E., Raaben,M., Wong,A.C., Herbert,A.S., Obernosterer,G., Mulherkar,N., Kuehne,A.I., Kranzusch,P.J., Griffin,A.M., Ruthel,G. *et al.* (2011) Ebola virus entry requires the cholesterol transporter Niemann–Pick C1. *Nature*, **477**, 340–343.
10. Birsoy,K., Wang,T., Possemato,R., Yilmaz,O.H., Koch,C.E., Chen,W.W., Hutchins,A.W., Gultekin,Y., Peterson,T.R., Carette,J.E. *et al.* (2012) MCT1-mediated transport of a toxic molecule is an effective strategy for targeting glycolytic tumors. *Nat. Genet.*, **45**, 104–108.
11. Tchasovnikarova,I.A., Timms,R.T., Matheson,N.J., Wals,K., Antrobus,R., Gottgens,B., Dougan,G., Dawson,M.A. and Lehner,P.J. (2015) Epigenetic silencing by the HUSH complex mediates position-effect variegation in human cells. *Science*, **348**, 1481–1485.
12. Essletzbichler,P., Konopka,T., Santoro,F., Chen,D., Gapp,B.V., Kralovics,R., Brummelkamp,T.R., Nijman,S.M.B. and Bürckstümmer,T. (2014) Megabase-scale deletion using CRISPR/Cas9 to generate a fully haploid human cell line. *Genome Res.*, **24**, 2059–2065.
13. Baggen,J., Thibaut,H.J., Staring,J., Jae,L.T., Liu,Y., Guo,H., Slager,J.J., de Bruin,J.W., van Vliet,A.L., Blomen,V.A. *et al.* (2016) Enterovirus D68 receptor requirements unveiled by haploid genetics. *Proc. Natl. Acad. Sci. U.S.A.*, **113**, 1399–1404.
14. Brockmann,M., Blomen,V.A., Nieuwenhuis,J., Stickel,E., Raaben,M., Bleijerveld,O.B., Altelaar,A.F.M., Jae,L.T. and Brummelkamp,T.R. (2017) Genetic wiring maps of single-cell protein states reveal an off-switch for GPCR signalling. *Nature*, **546**, 307–311.
15. Staring,J., von Castelmur,E., Blomen,V.A., van den Hengel,L.G., Brockmann,M., Baggen,J., Thibaut,H.J., Nieuwenhuis,J., Janssen,H., van Kuppeveld,F.J.M. *et al.* (2017) PLA2G16 represents a switch between entry and clearance of Picornaviridae. *Nature*, **541**, 412-416.
16. Evans,M.J. and Kaufman,M.H. (1981) Establishment in culture of pluripotential cells from mouse embryos. *Nature*, **292**, 154–156.
17. Martin,G.R. (1981) Isolation of a pluripotent cell line from early mouse embryos cultured in medium conditioned by teratocarcinoma stem cells. *Proc. Natl. Acad. Sci. U.S.A.*, **78**, 7634–7638.
18. Leeb,M. and Wutz,A. (2011) Derivation of haploid embryonic stem cells from mouse embryos. *Nature*, **479**, 131–134.
19. Elling,U., Taubenschmid,J., Wirnsberger,G., O'Malley,R., Demers,S.P., Vanhaelen,Q., Shukalyuk,A.I., Schmauss,G., Schramek,D., Schnuetgen,F. *et al.* (2011) Forward and reverse genetics through derivation of haploid mouse embryonic stem cells. *Cell Stem Cell*, **9**, 563–574.
20. Leeb,M., Walker,R., Mansfield,B., Nichols,J., Smith,A. and Wutz,A. (2012) Germline potential of parthenogenetic haploid mouse embryonic stem cells. *Development*, **139**, 3301–3305.
21. Pettitt,S.J., Rehman,F.L., Bajrami,I., Brough,R., Wallberg,F., Kozarewa,I., Fenwick,K., Assiotis,I., Chen,L., Campbell,J. *et al.* (2013) A genetic screen using the piggyBac transposon in haploid cells identifies Parp1 as a mediator of olaparib toxicity. *PLoS One*, **8**, e61520.
22. Leeb,M., Dietmann,S., Paramor,M., Niwa,H. and Smith,A. (2014) Genetic exploration of the exit from self-renewal using haploid embryonic stem cells. *Cell Stem Cell*, **14**, 385–393.
23. Monfort,A., Di Minin,G., Postlmayr,A., Freimann,R., Arieti,F., Thore,S. and Wutz,A. (2015) Identification of Spen as a crucial factor for Xist function through forward genetic screening in haploid embryonic stem cells. *Cell Rep.*, **12**, 554–561.
24. Pettitt,S.J., Krastev,D.B., Pemberton,H.N., Fontebasso,Y., Frankum,J., Rehman,F.L., Brough,R., Song,F., Bajrami,I., Rafiq,R. *et al.* (2017) Genome-wide barcoded transposon screen for cancer drug sensitivity in haploid mouse embryonic stem cells. *Sci. Data*, **4**, 170020.
25. Elling,U. and Penninger,J.M. (2014) Genome wide functional genetics in haploid cells. *FEBS Lett.*, **588**, 2415–2421.
26. Yang,H., Shi,L., Wang,B.A., Liang,D., Zhong,C., Liu,W., Nie,Y., Liu,J., Zhao,J., Gao,X. *et al.* (2012) Generation of genetically modified mice by oocyte injection of androgenetic haploid embryonic stem cells. *Cell*, **149**, 605–617.
27. Zhang,M., Liu,Y., Liu,G., Li,X., Jia,Y., Sun,L., Wang,L., Zhou,Q. and Huang,Y. (2015) Rapidly generating knockout mice from H19-Igf2 engineered androgenetic haploid embryonic stem cells. *Cell Discov.*, **1**, 15031.
28. Tucker,K.L., Wang,Y., Dausman,J. and Jaenisch,R. (1997) A transgenic mouse strain expressing four drug-selectable marker genes. *Nucleic Acids Res.*, **25**, 3745–3746.
29. Jackson,M., Taylor,A.H., Jones,E.A. and Forrester,L.M. (2010) The culture of mouse embryonic stem cells and formation of embryoid bodies. *Methods Mol. Biol.*, **633**, 1–18.
30. Li,M.A., Turner,D.J., Ning,Z., Yusa,K., Liang,Q., Eckert,S., Rad,L., Fitzgerald,T.W., Craig,N.L. and Bradley,A. (2011) Mobilization of giant piggyBac transposons in the mouse genome. *Nucleic Acids Res.*, **39**, e148.
31. Friedel,R.H., Friedel,C.C., Bonfert,T., Shi,R., Rad,R. and Soriano,P. (2013) Clonal expansion analysis of transposon insertions by high-throughput sequencing identifies candidate cancer genes in a PiggyBac mutagenesis screen. *PLos One*, **8**, e72338.
32. Schübeler,D., Yang,S.-H., Kalkan,T., Morrisroe,C., Smith,A. and Sharrocks,A.D. (2012) A genome-wide RNAi screen reveals MAP kinase phosphatases as key ERK pathway regulators during embryonic stem cell differentiation. *PLoS Genet.*, **8**, e1003112.
33. Cong,L., Ran,F.A., Cox,D., Lin,S., Barretto,R., Habib,N., Hsu,P.D., Wu,X., Jiang,W., Marraffini,L.A. *et al.* (2013) Multiplex genome engineering using CRISPR/Cas systems. *Science*, **339**, 819–823.
34. Ran,F.A., Hsu,P.D., Wright,J., Agarwala,V., Scott,D.A. and Zhang,F. (2013) Genome engineering using the CRISPR-Cas9 system. *Nat. Protoc.*, **8**, 2281–2308.
35. Ma,Y., Yao,N., Liu,G., Dong,L., Liu,Y., Zhang,M., Wang,F., Wang,B., Wei,X., Dong,H. *et al.* (2015) Functional screen reveals essential roles of miR-27a/24 in differentiation of embryonic stem cells. *EMBO J.*, **34**, 361–378.
36. Ran,F.A., Hsu,P.D., Lin,C.-Y., Gootenberg,J.S., Konermann,S., Trevino,A.E., Scott,D.A., Inoue,A., Matoba,S., Zhang,Y. *et al.* (2013) Double nicking by RNA-guided CRISPR Cas9 for enhanced genome editing specificity. *Cell*, **154**, 1380–1389.
37. Yamamizu,K., Fujihara,M., Tachibana,M., Katayama,S., Takahashi,A., Hara,E., Imai,H., Shinkai,Y. and Yamashita,J.K. (2012) Protein kinase A determines timing of early differentiation through epigenetic regulation with G9a. *Cell Stem Cell*, **10**, 759–770.
38. Caillier,M., Thenot,S., Tribollet,V., Birot,A.M., Samarut,J. and Mey,A. (2010) Role of the epigenetic regulator HP1gamma in the control of embryonic stem cell properties. *PLoS One*, **5**, e15507.
39. Wang,W., Bradley,A. and Huang,Y. (2009) A piggyBac transposon-based genome-wide library of insertionally mutated Blm-deficient murine ES cells. *Genome Res.*, **19**, 667–673.
40. Yusa,K., Zhou,L., Li,M.A., Bradley,A. and Craig,N.L. (2011) A hyperactive piggyBac transposase for mammalian applications. *Proc. Natl. Acad. Sci. U.S.A.*, **108**, 1531–1536.
41. Liang,Q., Kong,J., Stalker,J. and Bradley,A. (2009) Chromosomal mobilization and reintegration of Sleeping Beauty and piggyBac transposons. *Genesis*, **47**, 404–408.
42. Cadigan,K., Atlasi,Y., Noori,R., Gaspar,C., Franken,P., Sacchetti,A., Rafati,H., Mahmoudi,T., Decraene,C., Calin,G.A. *et al.*

(2013) Wnt signaling regulates the lineage differentiation potential of mouse embryonic stem cells through Tcf3 down-regulation. *PLoS Genet.*, **9**, e1003424.
43. Cole,M.F., Johnstone,S.E., Newman,J.J., Kagey,M.H. and Young,R.A. (2008) Tcf3 is an integral component of the core regulatory circuitry of embryonic stem cells. *Gene Dev.*, **22**, 746–755.
44. Mali,P., Yang,L., Esvelt,K.M., Aach,J., Guell,M., DiCarlo,J.E., Norville,J.E. and Church,G.M. (2013) RNA-guided human genome engineering via Cas9. *Science*, **339**, 823–826.
45. Smith,A. (2001) Embryo-derived stem cells: of mice and men. *Annu. Rev. Cell Dev. Biol.*, **17**, 435–462.
46. Ying,Q.-L., Stavridis,M., Griffiths,D., Li,M. and Smith,A. (2003) Conversion of embryonic stem cells into neuroectodermal precursors in adherent monoculture. *Nat. Biotechnol.*, **21**, 183–186.
47. Betschinger,J., Nichols,J., Dietmann,S., Corrin,P.D., Paddison,P.J. and Smith,A. (2013) Exit from pluripotency is gated by intracellular redistribution of the bHLH transcription factor Tfe3. *Cell*, **153**, 335–347.
48. McIlwain,D.R., Pan,Q., Reilly,P.T., Elia,A.J., McCracken,S., Wakeham,A.C., Itie-Youten,A., Blencowe,B.J. and Mak,T.W. (2010) Smg1 is required for embryogenesis and regulates diverse genes via alternative splicing coupled to nonsense-mediated mRNA decay. *Proc. Natl. Acad. Sci. U.S.A.*, **107**, 12186–12191.
49. Li,T., Shi,Y., Wang,P., Guachalla,L.M., Sun,B., Joerss,T., Chen,Y.S., Groth,M., Krueger,A., Platzer,M. *et al.* (2015) Smg6/Est1 licenses embryonic stem cell differentiation via nonsense-mediated mRNA decay. *EMBO J.*, **34**, 1630–1647.
50. Wang,C., Lee,J.E., Cho,Y.W., Xiao,Y., Jin,Q., Liu,C. and Ge,K. (2012) UTX regulates mesoderm differentiation of embryonic stem cells independent of H3K27 demethylase activity. *Proc. Natl. Acad. Sci. U.S.A.*, **109**, 15324–15329.
51. Maass,P.G., Aydin,A., Luft,F.C., Schächterle,C., Weise,A., Stricker,S., Lindschau,C., Vaegler,M., Qadri,F., Toka,H.R. *et al.* (2015) PDE3A mutations cause autosomal dominant hypertension with brachydactyly. *Nat. Genet.*, **47**, 647–653.
52. Fritz,A.L., Adil,M.M., Mao,S.R. and Schaffer,D.V. (2015) cAMP and EPAC signaling functionally replace OCT4 during induced pluripotent stem cell reprogramming. *Mol. Ther.*, **23**, 952–963.
53. Hou,P., Li,Y., Zhang,X., Liu,C., Guan,J., Li,H., Zhao,T., Ye,J., Yang,W., Liu,K. *et al.* (2013) Pluripotent stem cells induced from mouse somatic cells by small-molecule compounds. *Science*, **341**, 651–654.
54. Rodda,S.J., Kavanagh,S.J., Rathjen,J. and Rathjen,P.D. (2002) Embryonic stem cell differentiation and the analysis of mammalian development. *Int. J. Dev. Biol.*, **46**, 449–458.
55. Pommier,Y. (2013) Drugging topoisomerases: lessons and challenges. *ACS Chem. Biol.*, **8**, 82–95.
56. Mohr,S.E., Smith,J.A., Shamu,C.E., Neumuller,R.A. and Perrimon,N. (2014) RNAi screening comes of age: improved techniques and complementary approaches. *Nat. Rev. Mol. Cell Biol.*, **15**, 591–600.
57. Shalem,O., Sanjana,N.E. and Zhang,F. (2015) High-throughput functional genomics using CRISPR–Cas9. *Nat. Rev. Genet.*, **16**, 299–311.
58. Wu,X., Scott,D.A., Kriz,A.J., Chiu,A.C., Hsu,P.D., Dadon,D.B., Cheng,A.W., Trevino,A.E., Konermann,S., Chen,S. *et al.* (2014) Genome-wide binding of the CRISPR endonuclease Cas9 in mammalian cells. *Nat. Biotechnol.*, **32**, 670–676.
59. Pattanayak,V., Lin,S., Guilinger,J.P., Ma,E., Doudna,J.A. and Liu,D.R. (2013) High-throughput profiling of off-target DNA cleavage reveals RNA-programmed Cas9 nuclease specificity. *Nat. Biotechnol.*, **31**, 839–843.
60. Jackson,A.L., Bartz,S.R., Schelter,J., Kobayashi,S.V., Burchard,J., Mao,M., Li,B., Cavet,G. and Linsley,P.S. (2003) Expression profiling reveals off-target gene regulation by RNAi. *Nat. Biotechnol.*, **21**, 635–637.
61. Jae,L., Raaben,M., Riemersma,M., van Beusekom,E., Blomen,V., Velds,A., Kerkhoven,R., Carette,J., Topaloglu,H., Meinecke,P. *et al.* (2013) Deciphering the glycosylome of dystroglycanopathies using haploid screens for lassa virus entry. *Science*, **340**, 479–483.
62. Tafesse,F.G., Guimaraes,C.P., Maruyama,T., Carette,J.E., Lory,S., Brummelkamp,T.R. and Ploegh,H.L. (2014) GPR107, a G-protein-coupled receptor essential for Intoxication by pseudomonas aeruginosa exotoxin A, localizes to the Golgi and is cleaved by Furin. *J. Biol. Chem.*, **289**, 24005–24018.
63. Winter,G.E., Radic,B., Mayor-Ruiz,C., Blomen,V.A., Trefzer,C., Kandasamy,R.K., Huber,K.V., Gridling,M., Chen,D., Klampfl,T. *et al.* (2014) The solute carrier SLC35F2 enables YM155-mediated DNA damage toxicity. *Nat. Chem. Biol.*, **10**, 768–773.
64. Adams,R., Betz,H. and Püschel,A. (1996) A novel class of murine semaphorins with homology to thrombospondin is differentially expressed during early embryogenesis. *Mech. Dev.*, **57**, 33–45.
65. Simmons,A., Püschel,A., McPherson,J., Overhauser,J. and Lovett,M. (1998) Molecular cloning and mapping of human semaphorin F from the Cri-du-chat candidate interval. *Biochem. Biophys. Res. Commun.*, **242**, 685–691.
66. Fiore,R., Rahim,B., Christoffels,V.M., Moorman,A.F.M. and Puschel,A.W. (2005) Inactivation of the Sema5a gene results in embryonic lethality and defective remodeling of the cranial vascular system. *Mol. Cell. Biol.*, **25**, 2310–2319.
67. Iwase,S., Shono,N., Honda,A., Nakanishi,T., Kashiwabara,S., Takahashi,S. and Baba,T. (2006) A component of BRAF-HDAC complex, BHC80, is required for neonatal survival in mice. *FEBS Lett.*, **580**, 3129–3135.
68. Hailesellasse Sene,K., Porter,C.J., Palidwor,G., Perez-Iratxeta,C., Muro,E.M., Campbell,P.A., Rudnicki,M.A. and Andrade-Navarro,M.A. (2007) Gene function in early mouse embryonic stem cell differentiation. *BMC Genomics*, **8**, 85.
69. Bond,J., Roberts,E., Springell,K., Lizarraga,S., Scott,S., Higgins,J., Hampshire,D.J., Morrison,E.E., Leal,G.F., Silva,E.O. *et al.* (2005) A centrosomal mechanism involving CDK5RAP2 and CENPJ controls brain size. *Nat. Genet.*, **37**, 353–355.
70. Kraemer,N., Ravindran,E., Zaqout,S., Neubert,G., Schindler,D., Ninnemann,O., Gräf,R., Seiler,A.E.M. and Kaindl,A.M. (2015) Loss of Cdk5rap2 affects neural but not non-neural mESC differentiation into cardiomyocytes. *Cell Cycle*, **14**, 2044–2057.
71. Carette,J.E., Guimaraes,C.P., Wuethrich,I., Blomen,V.A., Varadarajan,M., Sun,C., Bell,G., Yuan,B., Muellner,M.K., Nijman,S.M. *et al.* (2011) Global gene disruption in human cells to assign genes to phenotypes by deep sequencing. *Nat. Biotechnol.*, **29**, 542–546.
72. Yilmaz,A., Peretz,M., Sagi,I. and Benvenisty,N. (2016) Haploid human embryonic stem cells: half the genome, double the value. *Cell Stem Cell*, **19**, 569–572.
73. Singh,T.R., Ali,A.M., Busygina,V., Raynard,S., Fan,Q., Du,C.H., Andreassen,P.R., Sung,P. and Meetei,A.R. (2008) BLAP18/RMI2, a novel OB-fold-containing protein, is an essential component of the Bloom helicase-double Holliday junction dissolvasome. *Genes Dev.*, **22**, 2856–2868.
74. Xu,D., Guo,R., Sobeck,A., Bachrati,C.Z., Yang,J., Enomoto,T., Brown,G.W., Hoatlin,M.E., Hickson,I.D. and Wang,W. (2008) RMI, a new OB-fold complex essential for Bloom syndrome protein to maintain genome stability. *Genes Dev.*, **22**, 2843–2855.
75. Hudson,D.F., Amor,D.J., Boys,A., Butler,K., Williams,L., Zhang,T. and Kalitsis,P. (2016) Loss of RMI2 increases genome instability and causes a bloom-like syndrome. *PLoS Genet.*, **12**, e1006483.
76. Walter,W., Thomalla,J., Bruhn,J., Fagan,D.H., Zehowski,C., Yee,D. and Skildum,A. (2015) Altered regulation of PDK4 expression promotes antiestrogen resistance in human breast cancer cells. *SpringerPlus*, **4**, 689.
77. Artunc,F., Nasir,O., Amann,K., Boini,K.M., Haring,H.U., Risler,T. and Lang,F. (2008) Serum- and glucocorticoid-inducible kinase 1 in doxorubicin-induced nephrotic syndrome. *Am. J. Physiol. Renal Physiol.*, **295**, F1624–F1634.
78. Walters,D.K., Steinmann,P., Langsam,B., Schmutz,S., Born,W. and Fuchs,B. (2008) Identification of potential chemoresistance genes in osteosarcoma. *Anticancer Res.*, **28**, 673–679.
79. Soupene,E., Kao,J., Cheng,D.H., Wang,D., Greninger,A.L., Knudsen,G.M., DeRisi,J.L. and Kuypers,F.A. (2016) Association of NMT2 with the acyl-CoA carrier ACBD6 protects the N-myristoyltransferase reaction from palmitoyl-CoA. *J. Lipid Res.*, **57**, 288–298.